Big city, small world: Density, contact rates, and transmission of dengue across Pakistan

Kraemer, M.U.G.*[1], Perkins, T. A.[2,3], Cummings, D.A.T.[4], Zakar, R.[5], Hay, S.I.[3,6,7], Smith, D.L.[1,3,8], and Reiner, R.C.*[3,9]

1. Department of Zoology, University of Oxford, Oxford, OX1 3PS, United Kingdom;
2. Department of Biological Sciences and Eck Institute for Global Health, University of Notre Dame, Notre Dame, IN 46556, United States;
3. Fogarty International Center, National Institutes of Health, Bethesda, MD 20892, United States;
4. Department of Epidemiology, Johns Hopkins University, Bloomberg School of Public Health, Baltimore, MD 21205, United States;
5. Department of Public Health, University of Punjab, Lahore, 54590, Pakistan;
6. Wellcome Trust Centre for Human Genetics, University of Oxford, Oxford, OX3 7BN, United Kingdom;
7. Institute for Health Metrics and Evaluation, University of Washington, Seattle, WA 98121, United States;
8. Sanaria Institute for Global Health and Tropical Medicine, Rockville, MD 20850, United States;
9. Department of Epidemiology and Biostatistics, Indiana University School of Public Health, Bloomington, IN 47405, United States;

* Author for correspondence: moritz.kraemer@zoo.ox.ac.uk or rcreiner@indiana.edu

Abstract:

Macroscopic descriptions of populations commonly assume that encounters between individuals are well mixed; i.e., each individual has an equal chance of coming into contact with any other individual. Relaxing this assumption can be challenging though, due to the difficulty of acquiring detailed knowledge about the non-random nature of encounters. Here, we fitted a mathematical model of dengue virus transmission to spatial time series data from Pakistan and compared maximum-likelihood estimates of "mixing parameters" when disaggregating data across an urban-rural gradient. We show that dynamics across this gradient are subject not only to differing transmission intensities but also to differing strengths of nonlinearity due to differences in mixing. We furthermore show that neglecting spatial variation in mixing can lead to substantial underestimates of the level of effort needed to control a pathogen with vaccines or other control efforts. We complement this analysis with relevant contemporary environmental drivers of dengue.

Keywords: dengue, epidemiology, heterogeneity, mixing, nonlinearity, spatial dynamics, vector-borne diseases, victim-exploiter dynamics

Introduction:

The transmission dynamics of all infectious diseases depend on a few basic but key determinants: the availability of susceptible and infectious hosts, contacts between them, and the potential for transmission upon contact. Susceptibility is shaped primarily by historical patterns of transmission, the natural history of the pathogen, the host's immune response, and host demography (Grenfell *et al.* 2004). What constitutes an epidemiologically significant contact depends on the pathogen's mode of transmission (Stoddard *et al.* 2009), and structure in contact patterns can be influenced by transportation networks and the spatial scale of transmission (Brockmann & Helbing 2013), by host heterogeneities such as age (Kilpatrick *et al.* 2006), and dynamically in response to the pathogen's influence on host behavior (Fenichel *et al.* 2011). Whether transmission actually occurs during contact between susceptible and infectious hosts often depends heavily on environmental conditions (Shaman *et al.* 2010; Gilbert *et al.* 2014; Weiss *et al.* 2014b). Disentangling the relative roles of these factors in driving patterns of disease incidence and prevalence is a difficult but central pursuit in infectious disease epidemiology, and mathematical models that are specific about the biology of how these mechanisms interact represent an indispensible tool in this pursuit (Anderson & May 1991).

The time-series susceptible-infected-recovered (TSIR) model was developed by Finkenstädt & Grenfell (2000) to offer a more accurate and straightforward way to statistically connect mechanistic models of infectious disease transmission with time series data. Among other features, TSIR models readily account for inhomogeneous mixing in a phenomenological way by allowing for nonlinear dependence of rates of contact between susceptible and infectious hosts on their densities. Although this is a simple feature that can be incorporated into any model based on mass-action assumptions – indeed, earlier applications pertained to inhomogeneous mixing in predator-prey systems (Pascual & Levin 1999) – the "mixing parameters" that determine the extent of this nonlinearity have primarily been fit to empirical data in applications of the TSIR model to transmission of measles, cholera, rubella, and dengue (Bjørnstad *et al.* 2002; Koelle & Pascual 2004; Metcalf *et al.* 2011; Reich *et al.* 2013). Applied to discrete-time models such as the TSIR, mixing parameters also have an interpretation as corrections for approximating a truly continuous-time process with a discrete-time model (Liu *et al.* 1987; Glass *et al.* 2003). In no application of the TSIR model to date has the potential for variation in these parameters been assessed, leaving the extent to which

inhomogeneity of mixing is different in space and time as an open question in the study of infectious disease dynamics.

There are a number of reasons why mixing might vary in time or space. Seasonal variation in mixing might arise because of travel associated with labor (Bharti *et al.* 2011), religious events (Lessler *et al.* 2014), or vacation (Deville *et al.* 2014). A major driver of flu is associated with the timing of school openings (Salathé *et al.* 2010), social networks (Cauchemez *et al.* 2011), and spatial variation in mixing could arise because of cultural differences and the geographic scales of interest (Brockmann & Helbing 2013; Vazquez-Prokopec *et al.* 2013; Read *et al.* 2014), because of variation in the density and quality of roads (Uchida & Nelson 2008), or because of variation in human densities and myriad factors associated with that (Bjørnstad *et al.* 2002; Simini *et al.* 2012). For vector-borne diseases, variation in mixing is amplified even further by variation in vector densities (Perkins *et al.* 2013), which effectively mediate contact between susceptible and infectious hosts.

Dengue is a mosquito-borne viral disease with a strong potential for spatial variation in mixing (Brady *et al.* 2012; Bhatt *et al.* 2013). The dominant vectors of dengue viruses (*Aedes spp.*) thrive in areas where they are able to associate with humans, as humans provide not only a preferred source of blood but also water containers that the mosquitoes use for egg laying and for larval and pupal development (Morrison *et al.* 2008). Two additional aspects of *Aedes* ecology – limited dispersal distance of the mosquito (Harrington *et al.* 2005) and daytime biting (Akram *et al.* 2009) – imply that human movement should be the primary means by which the viruses spread spatially (Stoddard *et al.* 2009). Indeed, analyses of dengue transmission dynamics at a variety of scales have strongly supported this hypothesis (Allicock *et al.* 2012; Stoddard *et al.* 2013; Bhoomiboonchoo *et al.* 2014; Reiner *et al.* 2014). To the extent that human movement in dense urban environments is more well-mixed than elsewhere, there are likely to be differences in the extent of inhomogeneous mixing in peri-urban and rural areas. This is also presumably the case for directly transmitted pathogens, but with a potentially even stronger discrepancy for dengue due to the urban-rural gradient in mosquito densities.

To assess the potential for spatial variation in the inhomogeneity of mixing as it pertains dengue transmission, we performed an analysis of district-level time series of dengue transmission in the Punjab province of Pakistan using a TSIR model with separate mixing parameters for urban and rural districts. We likewise made estimates of the relationships

between density-independent transmission potential and putative drivers thereof, such as temperature, to allow for the relative roles of extrinsic and intrinsic factors to be teased apart. Finally, we performed mathematical analyses of the fitted model to assess the significance of spatial variation in mixing inhomogeneity for how time series data are interpreted and used to guide control efforts.

Material and Methods:

We obtained daily dengue case data aggregated at hospital level from Punjab province provided by the Health Department Punjab, Pakistan between 2011 and 2014. In total, 41,300 suspected and confirmed dengue cases were reported in 109 hospitals. All hospitals were subsequently geo-located using 'Google maps' (http://www.maps.google.com). Hospitals that could not be identified were removed from the database. 21,182 cases alone were reported from the year 2011, which affected the almost the entire province. Many more cases occurred in Lahore (35,348) compared to all other districts (5,952) (Table 1). A breakdown per year and each province is provided in Table S1 and additional information about collection can be found in the supplementary appendix.

Covariate selection and processing:

Environmental conditions are instrumental in defining the risk of transmission of dengue (Bhatt *et al.* 2013). Transmission is limited by the availability of a competent disease vector. Due to a lack of resources and political instability no comprehensive nation wide entomological surveys have been performed in Pakistan. Therefore we use a probabilistic model to infer the probability of occurrence of *Ae. aegypti* and *Ae. albopictus* in Pakistan derived from a globally comprehensive dataset containing more than 20,000 records for each species (Figure 1a and b). Such model outputs have proven useful in identifying areas of risk of transmission of dengue as well as malaria (Gething *et al.* 2011; Sinka *et al.* 2012; Bhatt *et al.* 2013). Other important environmental conditions defining the risk of transmission of dengue are temperature, water availability, and vegetation cover (Messina *et al.* 2015). To account for such variation, raster layers of daytime land surface temperature (LST) were processed from the MOD11A2 satellite, gap-filled to remove missing values, and then averaged to a monthly temporal resolution for all four years (Weiss *et al.* 2015). The density of vegetation coverage has been shown to be associated with vector abundance (Eisen & Lozano-Fuentes 2009). Moreover, vegetation indices are useful proxies for precipitation and may be used to derive the

presence of standing water buckets that are habitats for the *Aedes* mosquitos (Maciel-de-Freitas *et al.* 2007). The same method was again applied to derive the Enhanced Vegetation Index (EVI) from the MOD11A2 satellite to produce 16 day and monthly pixel based estimates for 2011-2014 (Figure 1g) (Weiss *et al.* 2014a). Due to the inherent delay between rainfall and daily temperature influencing mosquito population dynamics and those mosquitoes contributing to an increase in DENV transmission, we consider both, the influence of the current temperature, vegetation indices and precipitation, data on current transmission as well as the values of those covariates the time step before (Figure 1f).

We used population count estimates on a 100m resolution that were subsequently aggregated up to match all other raster layers to a 5 km x 5 km resolution for the year 2015 (http://www.worldpop.org) (Figure 1e). In a follow-up analysis to our primary investigation into the climatological drivers of dengue transmission we included several density-based covariates. We derived a weighted accessibility metric that includes both, population density and urban accessibility, a metric commonly used to derive relative movement patterns (Uchida & Nelson 2008; Tatem *et al.* 2012). This map shows a friction surface, i.e. the time needed to travel through a specific pixel (Figure 1d). We also used an urban, peri-urban and rural classification scheme to quantify patterns of urbanicity based on a globally available grid (Center for International Earth Science Information Network (CIESIN) 2010) (Figure 1c). All covariates and case data were aggregated and averaged (where appropriate) to a district level.

Model:

Following Finkenstädt & Grenfell (2000), we assume a general transmission model of

$$I_{t,i} = \beta_{t,i} \cdot \frac{I_{t-1,i}^{\alpha_i}}{N_i} \cdot S_{t-1,i} \cdot \epsilon_{t,i}, \quad (1)$$

where $I_{t,i}$ is the number of infected and infectious individuals and $S_{t,i}$ the number of susceptible individuals, at time t in district i, N_i is the population of district i, and $\beta_{t,i}$ is the covariate driven contact rate. The mixing parameter for the ith district is given by α_i; when α_i is equal to 1, the population has homonegeous mixing where values less than one can either indicate inhomogeneous mixing or a need to correct for the discretization of the continuous-time process. Finally, the error terms $\epsilon_{t,i}$ are assumed to be independent and identically log-normally distributed random variables. For more details please see SI.

Model selection:

The term $\beta_{t,i}$ is fit using generalized additive model regression (GAM) (Hastie & Tibshirani 1990; Dominici *et al.* 2002; Wood 2011). The time-varying climatological covariates are all fit as a smooth spline, while all other covariates enter $\beta_{t,i}$ linearly. Additionally, unexplained seasonal variation is accounted for using a 12-month periodic smooth spline.

Model selection was performed using backwards selection. Two base models were investigated. First, a climate only model was created using only the climatological and climate suitability covariates. Second, a "full" model using the density-dependent covariates as well as the climatological covariates were combined into a single model which was then subjected to backwards selection. For both models the mixing coefficient was initially set equal for each district and once a final model was arrived upon, the mixing coefficient for Lahore was allowed to vary separately from the other coefficients. All model fitting was conducted using R (R Core Team 2014) and the "mgcv" package (Wood 2011). Models are fit by maximizing the restricted maximum likelihood (Patterson & Thompson 1971) to reduce bias and over-fitting of the smooth splines. The model source code and processing of covariates will be made available in line with previous projects (Pigott & Kraemer 2014).

Model analysis:

To explore the potential significance of spatial variation in mixing parameters, we conducted an analysis to probe the inherent mathematical tradeoff between the mixing parameter α and the density-independent transmission coefficient β. Specifically, to answer the question, what difference in local transmission would be necessary to account for a difference in mixing while achieving identical transmission dynamics. To explore this, we used eqn. (1) to establish:

$$\beta_1 \frac{{I_{1,t}}^{\alpha_1}}{N_1} = \beta_2 \frac{{I_{2,t}}^{\alpha_2}}{N_2} \qquad (2),$$

from which we obtained

$$\frac{\beta_1}{\beta_2} = I^{\alpha_2 - \alpha_1} \qquad (3).$$

We then examined how variation in *I* and $\alpha_2 - \alpha_1$ affected the left hand side of eqn. (3) and likewise the critical proportion of the population to control in order to effect pathogen elimination, which, under our model, is $p_c = 1 - \frac{1}{\beta}$.

Results:

Description of case distribution:

The majority of cases are clustered in Lahore, the capital of Punjab province. Ongoing transmission seems to be focal in three (Vehari, Rawlpindi and Lahore) districts and spread through infective sparks to smaller more rural provinces. In early investigations, all hospitals that reported dengue cases are located in areas with high EVI values indicating a clear environmental signal (Figure 1b).

Model selection:

To disentangle the different aspects of dengue dynamics and their drivers we used a model containing only the climatological covariates and performing backwards model selection until each covariate in the model was significant at a 5% level resulted in a model that explained 76.9% of the deviance and whose adjusted R-squared was 0.746. Amongst the yearly-averaged covariates, EVI and precipitation remained in the model as well as the derived *Ae. albopictus* range map (p-values of 8.21×10^{-4}, 0.01, and 3.9×10^{-5} respectively). Interestingly, if the derived *Ae. aegypti* map is substituted for the *Ae. albopictus* map, the deviance explained increases slightly to 76.8%. For climatological covariates that were fit as smooth splines, temperature, lagged temperature and EVI remained in the model (Figure 2, p-values of 0.010, 0.030 and 0.030 with effective degrees of freedom 7.55, 5.47, and 1.83, respectively). There was a significant amount of periodic variation unexplained by the climatological covariates alone and the 'seasonality' covariate remained (Figure 2, p-value = 0.0034). The estimated median values for R_0 per district are clustered around two (mean = 2.1), their geographical distribution indicates a clear trend towards districts with higher population (Figure 3). Finally, the mixing coefficient was significantly lower than 1 ($\alpha = 0.69$, 95% CI = (0.614, 0.771), p-value $= 1.6\ x\ 10^{-14}$).

To understand these differences the final model was then compared to a nested model where the coefficient for Lahore was allowed to vary independently of all other districts. Deviance explained increased to 77% and adjusted R-squared increased to 0.753. Further, the mixing coefficient for Lahore ($\alpha = 0.74$) was significantly larger than the mixing coefficient for the other districts ($\alpha = 0.59$, p-value=0.0068) (Figure S1). The median R_0 for Lahore was estimated at 3.28, the highest for all districts.

In assess how far the variation of mixing coefficients can be explained by other covariates we consider the possibility that movement accounts for the differences in the mixing coefficient between Lahore and the other districts. The density-dependent covariates (described earlier)

were then added to the full model and backwards selection was repeated. The resulting model explained 78.6% of the variance, had an adjusted R-squared of 0.763 and is superior to the final climatological model based on AIC (699.23 versus 714.83). Yearly averaged EVI, NDVI and precipitation were all significant (p-values of 8.7×10^{-5}, 0.00024, and 0.00028, respectively). Again, the derived *Ae. albopictus* map was significant (p-value = 0.008163). For climatological covariates fit as smooth splines, only temperature and lagged temperature were found significant (Figure 2b, p-value of 4.0×10^{-5} and 0.0013, and effective degrees of freedom 7.61 and 4.81, respectively), and there was still a significant 'seasonality' (Figure 2b, p-value of 4.0×10^{-7}, effective degrees of freedom 4.48). The mixing coefficient was fit at $\alpha = 0.58$, barely lower than the mixing coefficient for non-Lahore districts in the climatological model. The estimated median R_0 again clustered around 2 (mean = 1.8), and again the R_0 for Lahore was largest, but in this model it was considerably larger than in the climatological model (Lahore R_0 = 7.82, Figure 2b). Full details of the model parameters are shown in Table S2-S5.

Two of the density-dependent covariates remained in the model: the urban map (p-value = 0.01) and the weighted access map (p-value= 3×10^{-5}). When the nested model that allows Lahore's mixing coefficient to vary was fit, there was no significant difference in the two mixing coefficients (p-value$\approx$1).

Model analysis:

Given a difference in estimates of the mixing parameters between Lahore and elsewhere of 0.15, we analyzed eqn. (3) to assess the bias in estimates of the transmission coefficient that would result from ignoring this extent of variation in the inhomogeneity of mixing displayed between two areas. For the purpose of *ceteris paribus* comparisons, we assumed equal force of infection but varied it across several orders of magnitude. Depending on the order of magnitude, estimates of transmission coefficients made if overestimating the mixing parameter by 0.15 could easily result in a two- to three-fold underestimate in the transmission coefficient (Figure 4). For realistic ranges of the transmission coefficient for dengue, and more generally the basic reproductive number R_0, this extent of underestimation of R_0 could lead to underestimating the critical proportion of the population to which vaccines or other control measures must be applied by 20-30% (Figure 5).

Discussion:

Our results point to considerable spatial heterogeneity in the extent of mixing and strength of an associated nonlinearity in transmission along an urban-rural gradient. This regional variability in mixing has direct implications for estimates of the basic reproductive number of dengue in our study region and elsewhere. Although the potential for such bias in estimates of the basic reproductive number has been shown in a theoretical context (Hu *et al.* 2013; Perkins *et al.* 2013), we provide quantitative estimates of the extent of this problem in interfacing models with a rich spatio-temporal data set. Such analyses have implications for estimates of population-level parameters not only for dengue but also for other infectious diseases (Bartlett 1960; Keeling & Grenfell 1997; Bjørnstad *et al.* 2002; Smith *et al.* 2002; Keeling & Eames 2005; Kiss *et al.* 2008) and possibly even more broadly in ecology.

We revealed significant differences in mixing components between urban and rural settings and found that a population-weighted urban accessibility metric was able to absorb differences in mixing between these settings indicating that this specific covariate accounts for aspects influencing mixing. Mixing is presumably influenced directly by human behavior and has been shown to be highly unpredictable, largely dependent on the local context and the spatial and temporal scale (Yang *et al.* 2014). In this study however we could show that the density-dependent covariate selected was able to capture the influence of these key encounters on a district level. Once differences in mixing were accounted for, estimated R_0 values indicated considerably larger differences between transmission potential in Lahore versus all other districts. Synchronizing more accurate geo-referenced data would allow to assess the importance of spatial scale on the relationship between “mixing parameters” and urban accessibility (Perkins *et al.* 2013; Mills & Riley 2014). In the case of dengue this again has been limited by the availability of high resolution data (Ruberto *et al.* 2015). Complementing this analysis with measurement of direct social contact patterns could be important to explore this relationship in even more detail (Bauch & Galvani 2013; Vazquez-Prokopec *et al.* 2013; Heesterbeek *et al.* 2015) and could be informed by mathematical models that explored this relationship previously for other diseases (Bjørnstad *et al.* 2002; Reiner *et al.* 2012). Another encouraging finding is that large-scale mosquito suitability surfaces help capture the environmental determinants of dengue transmission (Bhatt *et al.* 2013).

Intervention strategies are contingent on both understanding key environmental drivers of transmission and the dynamics of ongoing human-to-human transmission, particularly in outbreaks situations (Perkins *et al.* 2015). Environmental drivers such as seasonal fluctuations

312 in rainfall, temperature, vegetation coverage or mosquito abundance will help guide
313 surveillance and control efforts targeted mostly towards the ecological aspects of mosquito
314 dispersal (Johansson 2015). Once infection occurs much debate has been focused around
315 optimizing intervention strategies to reduce disease incidence, which is largely determined by
316 R_0. The presented framework shows that the interaction between mixing parameters and force
317 of infection has potentially large implications for optimizing targeted intervention, particularly in
318 countries where resources are scarce (Cesare *et al.* 2015). This in fact is even more important
319 in areas of low infection where transmission seems to be more focal (Salje *et al.* 2012). Again
320 however importance needs to be focused on the spatial and temporal resolution of appropriate
321 intervention strategies and the respective effect of the selected covariates and model
322 parameters (Mills & Riley 2014). Empirical understanding, however, on which spatial resolution
323 is most appropriate to carry out large-scale vector-borne disease interventions remains
324 unknown.
325
326 Once transmission has occurred in one place, understanding not only spatial heterogeneities of
327 transmission dynamics but their subsequent spread in mechanistic stochastic models as shown
328 for measles would help to empirically determine the propagation of the disease (Grenfell *et al.*
329 2001). The spatial spread dynamics have been given considerable interest globally as the risk
330 of importation of dengue into yet endemic areas continentally and internationally is increasing
331 with travel and trade (Schaffner & Mathis 2014). Exploration of the case data in Pakistan
332 suggests that spread happens along major transport routes from Lahore to Karachi and north
333 to Rawalpindi. Using results presented here on mixing components and environmental drivers
334 will help pinpoint areas of major risk of importation more accurately especially in the case of
335 recurring epidemics. Using the fitted relationships of the environmental drivers of transmission
336 and R_0 will enable future analyses and comparisons between diseases and geographic regions.
337 In this context it will be instrumental to integrate a variety of movement and social network
338 models with the evidence presented here to infer more accurately how the geographical spread
339 of dengue is determined.
340
341 To allow for comparison of these results in a broader context and across diseases, possibly
342 even in outbreak situations and in real time, it is essential to make data widely available by
343 open access (Heesterbeek *et al.* 2015). Moreover, the complexity of infectious disease
344 dynamics is not fully understood and we are limited by computational capacities to fully account
345 for stochasticity and nonlinearity.

346
347 **Author contributions:**
348 Conceived and designed the experiment: MUGK, RCR, TAP, DLS. Performed the experiments:
349 RCR, TAP, MUGK. Analysed the data: RCR, MUGK. Edited the manuscript: DLS, SIH, DATC,
350 ZR. Wrote the paper: MUGK, RCR, TAP.
351
352 **Acknowledgements and funding:**
353
354 The authors would like to thank the WHO Punjab office, Health Department Punjab, and PID
355 for providing the epidemiological data, and all participants that helped collect the data. MUGK
356 acknowledges funding from the German Academic Exchange Service (DAAD). TAP, SIH, RCR
357 acknowledge the support from the RAPIDD program of the Science & Technology Directorate,
358 Department of Homeland Security, and the Fogarty International Center, National Institutes of
359 Health. SIH is funded by a Senior Research Fellowship from the Wellcome Trust (#095066)
360 and a grant from the Bill & Melinda Gates Foundation (#OPP1093011). Funders had no role in
361 study design, data collection and analysis, decision to publish, or preparation of the
362 manuscript.
363
364
365 **References:**
366 1.
367 Akram, W., Hafeez, F., Ullah, U.N., Kim, Y.K., Hussain, A. & Lee, J.J. (2009). Seasonal
368 distribution and species composition of daytime biting mosquitoes. *Entomol. Res.*, 39, 107–13.
369 2.
370 Allicock, O.M., Lemey, P., Tatem, A.J., Pybus, O.G., Bennett, S.N., Mueller, B. a., *et al.* (2012).
371 Phylogeography and population dynamics of dengue viruses in the Americas. *Mol. Biol. Evol.*,
372 29, 1533–43.
373 3.
374 Anderson, R.M. & May, R.M. (1991). *Infectious diseases of humans: dynamics and control*.
375 Oxford University Press, Oxford, U.K.
376 4.
377 Bartlett, M.S. (1960). The critical community size for measles in the U.S. *J. R. Stat. Soc. A*,
378 123, 37–44.
379 5.
380 Bauch, C.T. & Galvani, A.P. (2013). Epidemiology. Social factors in epidemiology. *Science*,
381 342, 47–9.
382 6.
383 Bharti, N., Tatem, a J., Ferrari, M.J., Grais, R.F., Djibo, A. & Grenfell, B.T. (2011). Explaining
384 seasonal fluctuations of measles in Niger using nighttime lights imagery. *Science*, 334, 1424–7.
385 7.
386 Bhatt, S., Gething, P.W., Brady, O.J., Messina, J.P., Farlow, A.W., Moyes, C.L., *et al.* (2013).
387 The global distribution and burden of dengue. *Nature*, 496, 504–7.
388 8.
389 Bhoomiboonchoo, P., Gibbons, R. V., Huang, A., Yoon, I.-K., Buddhari, D., Nisalak, A., *et al.*
390 (2014). The spatial dynamics of Dengue virus in Kamphaeng Phet, Thailand. *PLoS Negl. Trop.*
391 *Dis.*, 8, e3138.
392 9.
393 Bjørnstad, O.N., Finkenstädt, B.F. & Grenfell, B.T. (2002). Dynamics of measles epidemics:
394 Estimating scaling of transmission rates using a Time Series SIR model. *Ecol. Monogr.*, 72,
395 169–84.

10.
Brady, O.J., Gething, P.W., Bhatt, S., Messina, J.P., Brownstein, J.S., Hoen, A.G., *et al.* (2012). Refining the global spatial limits of dengue virus transmission by evidence-based consensus. *PLoS Negl. Trop. Dis.*, 6, e1760.
11.
Brockmann, D. & Helbing, D. (2013). The hidden geometry of complex, network-driven contagion phenomena. *Science*, 342, 1337–42.
12.
Cauchemez, S., Bhattarai, A., Marchbanks, T.L., Fagan, R.P., Ostroff, S., Ferguson, N.M., *et al.* (2011). Role of social networks in shaping disease transmission during a community outbreak of 2009 H1N1 pandemic influenza. *Proc. Natl. Acad. Sci.*, 108, 2825–30.
13.
Center for International Earth Science Information Network (CIESIN). (2010). *Gridded Population of the World, version 3 (GPWv3) and the Global Rural-Urban Mapping Project (GRUMP)*.
14.
Cesare, M. Di, Bhatti, Z., Soofi, S.B., Fortunato, L., Ezzati, M. & Bhutta, Z. a. (2015). Geographical and socioeconomic inequalities in women and children's nutritional status in Pakistan in 2011: an analysis of data from a nationally representative survey. *Lancet Glob. Heal.*, 3, e229–39.
15.
Deville, P., Linard, C., Martin, S., Gilbert, M., Stevens, F.R., Gaughan, a. E., *et al.* (2014). Dynamic population mapping using mobile phone data. *Proc. Natl. Acad. Sci.*, 111, 15888–93.
16.
Dominici, F., McDermott, A., Zeger, S.L. & Samet, J.M. (2002). On the use of generalized additive models in time-series studies of air pollution and health. *Am. J. Epidemiol.*, 156, 193–203.
17.
Eisen, L. & Lozano-Fuentes, S. (2009). Use of mapping and spatial and space-time modeling approaches in operational control of Aedes aegypti and dengue. *PLoS Negl. Trop. Dis.*, 3, e411.
18.
Fenichel, E.P., Castillo-Chavez, C., Ceddia, M.G., Chowell, G., Parra, P. a G., Hickling, G.J., *et al.* (2011). Adaptive human behavior in epidemiological models. *Proc. Natl. Acad. Sci.*, 108, 6306–11.
19.
Finkenstädt, B.F. & Grenfell, B.T. (2000). Time series modelling of childhood diseases: a dynamical systems approach. *Appl. Stat.*, 49, 187–205.
20.
Gething, P.W., Patil, A.P., Smith, D.L., Guerra, C. a, Elyazar, I.R.F., Johnston, G.L., *et al.* (2011). A new world malaria map: Plasmodium falciparum endemicity in 2010. *Malar. J.*, 10, 378.
21.
Gilbert, M., Golding, N., Zhou, H., Wint, G.R.W., Robinson, T.P., Tatem, A.J., *et al.* (2014). Predicting the risk of avian influenza A H7N9 infection in live-poultry markets across Asia. *Nat. Commun.*, 5, 4116.
22.
Glass, K., Xia, Y. & Grenfell, B.T. (2003). Interpreting time-series analyses for continuous-time biological models - Measles as a case study. *J. Theor. Biol.*, 223, 19–25.
23.

446 Grenfell, B.T., Bjùrnstad, O.N. & Kappey, J. (2001). Travelling waves and spatial hierarchies in
447 measles epidemics. *Nature*, 414, 716–23.
448 24.
449 Grenfell, B.T., Pybus, O.G., Gog, J.R., Wood, J.L.N., Daly, J.M., Mumford, J. a, *et al.* (2004).
450 Unifying the epidemiological and evolutionary dynamics of pathogens. *Science*, 303, 327–32.
451 25.
452 Harrington, L.C., Scott, T.W., Lerdthusnee, K., Coleman, R.C., Costero, A., Clark, G.G., *et al.*
453 (2005). Dispersal of the dengue vector Aedes aegypti within and between rural communities.
454 *Am. J. Trop. Med. Hyg.*, 72, 209–20.
455 26.
456 Hastie, T.J. & Tibshirani, R.J. (1990). *Generalized additive models*. Vol. 43. CRC Press.
457 27.
458 Heesterbeek, H., Anderson, R.M., Andreasen, V., Bansal, S., De Angelis, D., Dye, C., *et al.*
459 (2015). Modeling infectious disease dynamics in the complex landscape of global health.
460 *Science*, 347, aaa4339.
461 28.
462 Hu, H., Nigmatulina, K. & Eckhoff, P. (2013). The scaling of contact rates with population
463 density for the infectious disease models. *Math. Biosci.*, 244, 125–34.
464 29.
465 Johansson, M.A. (2015). Chikungunya on the move. *Trends Parasitol.*, 31, 43–45.
466 30.
467 Keeling, M.J. & Eames, K.T.D. (2005). Networks and epidemic models. *J. R. Soc. Interface*, 2,
468 295–307.
469 31.
470 Keeling, M.J. & Grenfell, B.T. (1997). Disease extinction and community size: modeling the
471 persistence of measles. *Science*, 275, 65–7.
472 32.
473 Kilpatrick, A.M., Daszak, P., Jones, M.J., Marra, P.P. & Kramer, L.D. (2006). Host
474 heterogeneity dominates West Nile virus transmission. *Proc. Biol. Sci.*, 273, 2327–33.
475 33.
476 Kiss, I.Z., Green, D.M. & Kao, R.R. (2008). The effect of network mixing patterns on epidemic
477 dynamics and the efficacy of disease contact tracing. *J. R. Soc. Interface*, 5, 791–9.
478 34.
479 Koelle, K. & Pascual, M. (2004). Disentangling extrinsic from intrinsic factors in disease
480 dynamics: A nonlinear time series approach with an application to Cholera. *Am. Nat.*, 163,
481 901–13.
482 35.
483 Lessler, J., Rodriguez, I., Derek, B., Tini, A.T.C., Kerkhove, M. Van, Mills, H., *et al.* (2014).
484 Estimating potential incidence of MERS CoV associated with Hajj pilgrims to Saudi Arabia,
485 2014. *PLOS Curr. Outbreaks*, November 2.
486 36.
487 Liu, W.M., Hethcote, H.W. & Levin, S. a. (1987). Dynamical behavior of epidemiological models
488 with nonlinear incidence rates. *J. Math. Biol.*, 25, 359–380.
489 37.
490 Maciel-de-Freitas, R., Marques, W. a., Peres, R.C., Cunha, S.P. & De Oliveira, R.L. (2007).
491 Variation in Aedes aegypti (Diptera: Culicidae) container productivity in a slum and a suburban
492 district of Rio de Janeiro during dry and wet seasons. *Mem. Inst. Oswaldo Cruz*, 102, 489–96.
493 38.
494 Messina, J.P., Brady, O.J., Pigott, D.M., Golding, N., Kraemer, M.U.G., Scott, T.W., *et al.*
495 (2015). The many projected futures of dengue. *Nat. Rev. Microbiol.*, 13, 230–39.

496 39.
497 Metcalf, C.J.E., Bjornstad, O.N., Ferrari, M.J., Klepac, P., Bharti, N., Lopez-Gatell, H., *et al.*
498 (2011). The epidemiology of rubella in Mexico: seasonality, stochasticity and regional variation.
499 *Epidemiol. Infect.*, 139, 1029–38.
500 40.
501 Mills, H.L. & Riley, S. (2014). The spatial resolution of epidemic peaks. *PLoS Comput. Biol.*, 10,
502 e1003561.
503 41.
504 Morrison, A.C., Zielinski-Gutierrez, E., Scott, T.W. & Rosenberg, R. (2008). Defining challenges
505 and proposing solutions for control of the virus vector Aedes aegypti. *PLoS Med.*, 5, e68.
506 42.
507 Pascual, M. & Levin, S. a. (1999). From individuals to population densities: searching for the
508 scale of intermediate determinism. *Ecology*, 80, 2225–36.
509 43.
510 Patterson, H.D. & Thompson, R. (1971). Recovery of inter-block information when block sizes
511 are unequal. *Biometrika*, 58, 545–54.
512 44.
513 Perkins, T.A., Metcalf, C.J.E., Grenfell, B.T. & Tatem, A.J. (2015). Estimating Drivers of
514 Autochthonous Transmission of Chikungunya Virus in its Invasion of the Americas. *PLoS Curr.*,
515 7, ecurrents.outbreaks.a4c7b6ac10e0420b1788c9767946d1.
516 45.
517 Perkins, T.A., Scott, T.W., Le Menach, A. & Smith, D.L. (2013). Heterogeneity, mixing, and the
518 spatial scales of mosquito-borne Ppathogen transmission. *PLoS Comput. Biol.*, 9, e1003327.
519 46.
520 Pigott, D.M. & Kraemer, M.U. (2014). Enhancing infectious disease mapping with open access
521 resources. *Eurosurveillance*, 19, pii=20989.
522 47.
523 R Core Team. (2014). R: A language and environment for computing. Vienna, Austria. *R*
524 *Found. Stat. Comput.*
525 48.
526 Read, J.M., Lessler, J., Riley, S., Wang, S., Tan, L.J., Kwok, K.O., *et al.* (2014). China social
527 mixing patterns in rural and urban areas of southern China. *Proc. R. Soc. B*, 281, 20140268.
528 49.
529 Reich, N.G., Shrestha, S., King, A. a, Rohani, P., Lessler, J., Kalayanarooj, S., *et al.* (2013).
530 Interactions between serotypes of dengue highlight epidemiological impact of cross-immunity.
531 *J. R. Soc. Interface*, 10, 20130414.
532 50.
533 Reiner, R.C., King, A. a, Emch, M., Yunus, M., Faruque, a S.G. & Pascual, M. (2012). Highly
534 localized sensitivity to climate forcing drives endemic cholera in a megacity. *Proc. Natl. Acad.*
535 *Sci.*, 109, 2033–6.
536 51.
537 Reiner, R.C., Stoddard, S.T. & Scott, T.W. (2014). Socially structured human movement
538 shapes dengue transmission despite the diffusive effect of mosquito dispersal. *Epidemics*, 6,
539 30–6.
540 52.
541 Ruberto, I., Marques, E., Burke, D.S. & Van Panhuis, W.G. (2015). The availability and
542 consistency of dengue surveillance data Pprovided online by the World Health Organization.
543 *PLoS Negl. Trop. Dis.*, 9, e0003511.
544 53.

545 Salathé, M., Kazandjieva, M., Woo, J., Levis, P., Feldman, M.W. & Jones, J.H. (2010). A high-
546 resolution human contact network for infectious disease transmission. *Proc. Natl. Acad. Sci.*,
547 107, 22020–5.
548 54.
549 Salje, H., Lessler, J., Endy, T.P., Curriero, F.C., Gibbons, R. V., Nisalak, A., *et al.* (2012).
550 Revealing the microscale spatial signature of dengue transmission and immunity in an urban
551 population. *Proc. Natl. Acad. Sci.*, 109, 9535–8.
552 55.
553 Schaffner, F. & Mathis, A. (2014). Dengue and dengue vectors in the WHO European region:
554 past, present, and scenarios for the future. *Lancet. Infect. Dis.*, 14, 1271–80.
555 56.
556 Shaman, J., Pitzer, V.E., Viboud, C., Grenfell, B.T. & Lipsitch, M. (2010). Absolute humidity and
557 the seasonal onset of influenza in the continental United States. *PLoS Biol.*, 8.
558 57.
559 Simini, F., González, M.C., Maritan, A. & Barabási, A.-L. (2012). A universal model for mobility
560 and migration patterns. *Nature*, 484, 96–100.
561 58.
562 Sinka, M.E., Bangs, M.J., Manguin, S., Rubio-Palis, Y., Chareonviriyaphap, T., Coetzee, M., *et*
563 *al.* (2012). A global map of dominant malaria vectors. *Parasit. Vectors*, 5, 69.
564 59.
565 Smith, D.L., Lucey, B., Waller, L. a, Childs, J.E. & Real, L. a. (2002). Predicting the spatial
566 dynamics of rabies epidemics on heterogeneous landscapes. *Proc. Natl. Acad. Sci.*, 99, 3668–
567 72.
568 60.
569 Stoddard, S.T., Forshey, B.M., Morrison, A.C., Paz-Soldan, V. a, Vazquez-Prokopec, G.M.,
570 Astete, H., *et al.* (2013). House-to-house human movement drives dengue virus transmission.
571 *Proc. Natl. Acad. Sci.*, 110, 994–9.
572 61.
573 Stoddard, S.T., Morrison, A.C., Vazquez-Prokopec, G.M., Paz Soldan, V., Kochel, T.J., Kitron,
574 U., *et al.* (2009). The role of human movement in the transmission of vector-borne pathogens.
575 *PLoS Negl. Trop. Dis.*, 3.
576 62.
577 Tatem, A.J., Hemelaar, J., Gray, R.R. & Salemi, M. (2012). Spatial accessibility and the spread
578 of HIV-1 subtypes and recombinants. *AIDS*, 26, 2351–60.
579 63.
580 Uchida, H. & Nelson, A. (2008). *Agglomeration index: towards a new measure of urban*
581 *concentration*. Washington D.C.
582 64.
583 Vazquez-Prokopec, G.M., Bisanzio, D., Stoddard, S.T., Paz-Soldan, V., Morrison, A.C., Elder,
584 J.P., *et al.* (2013). Using GPS technology to quantify human mobility, dynamic contacts and
585 infectious disease dynamics in a resource-poor urban environment. *PLoS One*, 8, e58802.
586 65.
587 Weiss, D.J., Atkinson, P.M., Bhatt, S., Mappin, B., Hay, S.I. & Gething, P.W. (2014a). An
588 effective approach for gap-filling continental scale remotely sensed time-series. *ISPRS J.*
589 *Photogramm. Remote Sens.*, 98, 106–18.
590 66.
591 Weiss, D.J., Bhatt, S., Mappin, B., Van Boeckel, T.P., Smith, D.L., Hay, S.I., *et al.* (2014b). Air
592 temperature suitability for Plasmodium falciparum malaria transmission in Africa 2000-2012: a
593 high-resolution spatiotemporal prediction. *Malar. J.*, 13, 171.
594 67.

595 Weiss, D.J., Mappin, B., Dalrymple, U., Bhatt, S., Cameron, E., Hay, S.I., *et al.* (2015). Re-
596 examining environmental correlates of Plasmodium falciparum malaria endemicity: a data-
597 intensive variable selection approach. *Malar. J.*, 14, 1–18.
598 68.
599 Wood, S.N. (2011). Fast stable restricted maximum likelihood and marginal likelihood
600 estimation of semiparametric generalized linear models. *J. R. Stat. Soc. Ser. B Stat. Methodol.*,
601 73, 3–36.
602 69.
603 Yang, Y., Herrera, C., Eagle, N. & González, M.C. (2014). Limits of predictability in commuting
604 flows in the absence of data for calibration. *Sci. Rep.*, 4, 5662.
605

606 **Table 1: Reported cases by year in Lahore and all other districts.**

	2011	2012	2013	2014	Total
Lahore	18,020	4,013	11,516	1,799	35,348
Other	3,162	500	2,356	2,790	5,952

607

608 **Figure 1: Covariates used in this study to derive environmental drivers of transmission.**
609 ***Aedes aegypti* probability of occurrence (a); *Ae. albopictus* probability of occurrence**
610 **(b); Urbanicity (c); Weighted urban accessibility (d); Population density and study area**
611 **(e); Precipitation (f); Enhanced Vegetation Index (EVI) mean (g).**

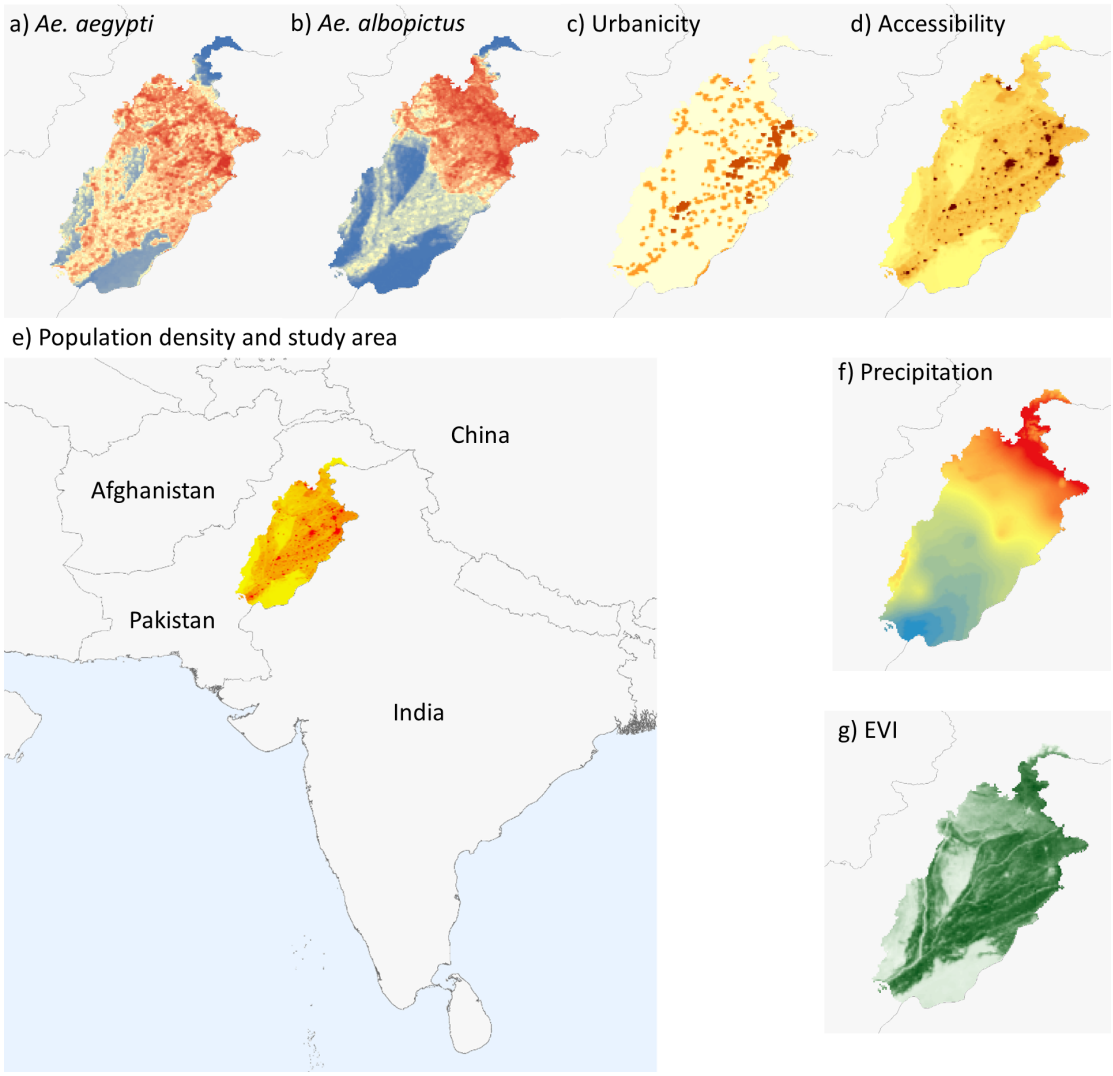

612

613

614 **Figure 2: Model outputs using a backwards model selection procedure in the model**
615 **using climatological variables (a, A-D), and including the density dependent variables (b,**
616 **A-D).**

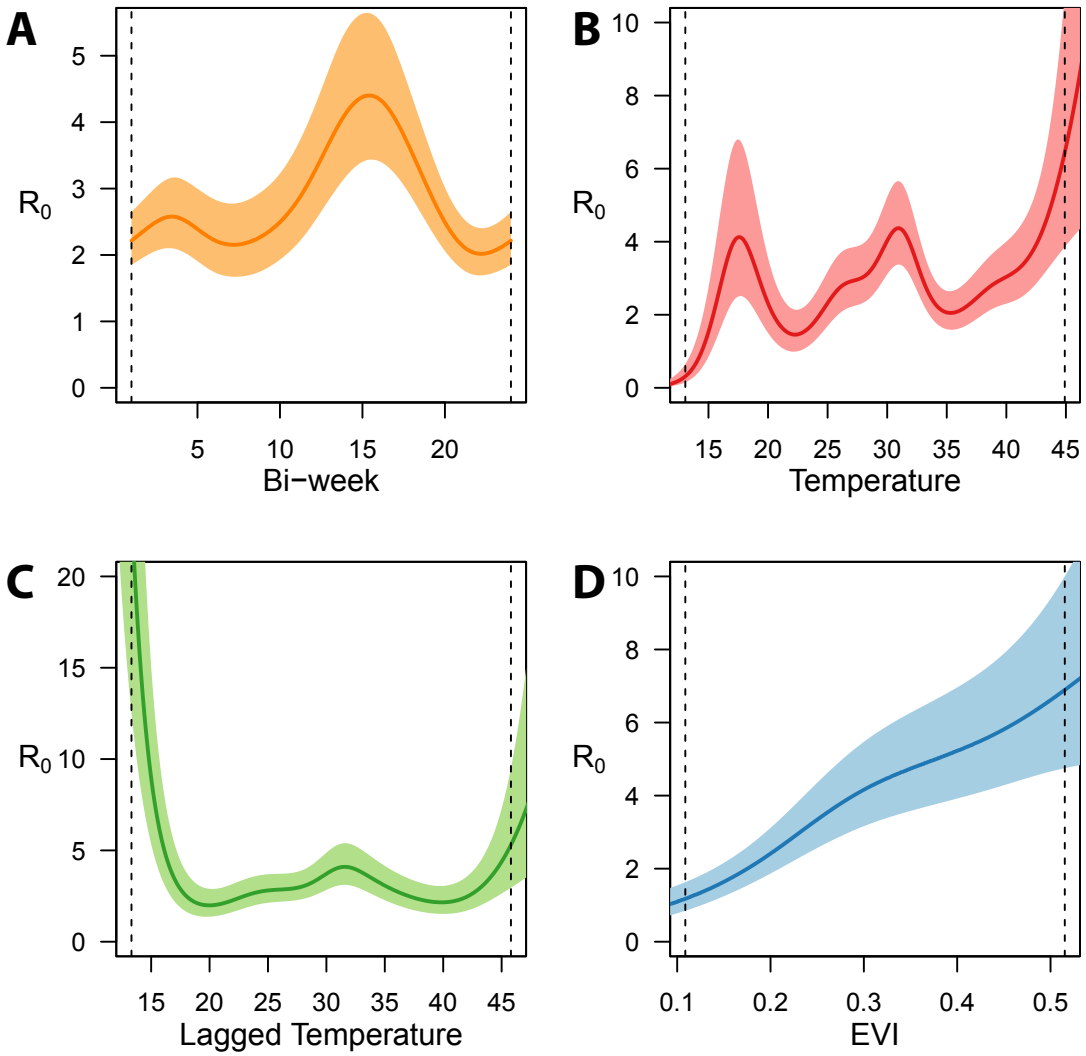

617

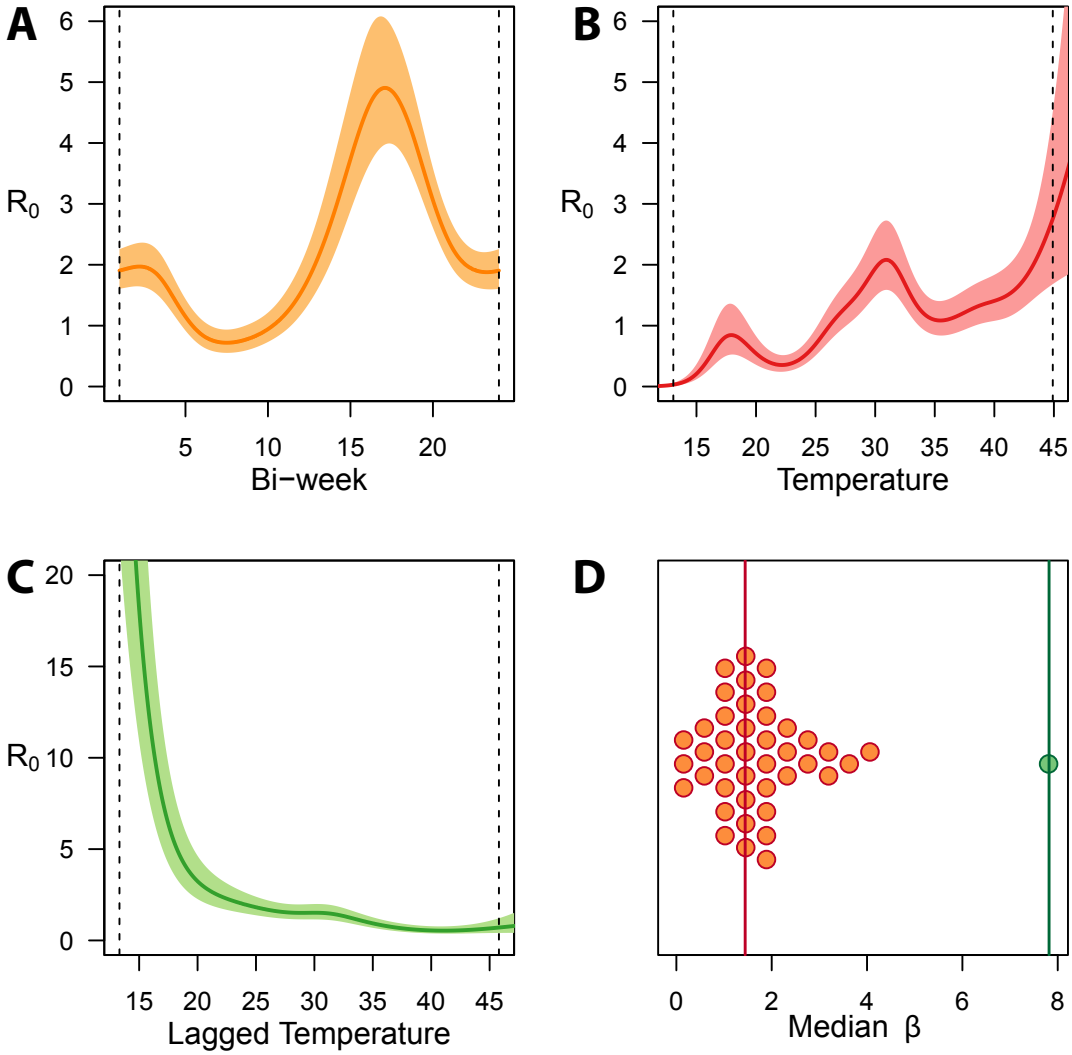

618

619

620

621

622 **Figure 3: Average distribution of R_0 with green representing Lahore versus red all other**
623 **districts (A), their geographical distribution (B), and over time in which the green line**
624 **again is representing Lahore versus the red line representing all other districts (C).**

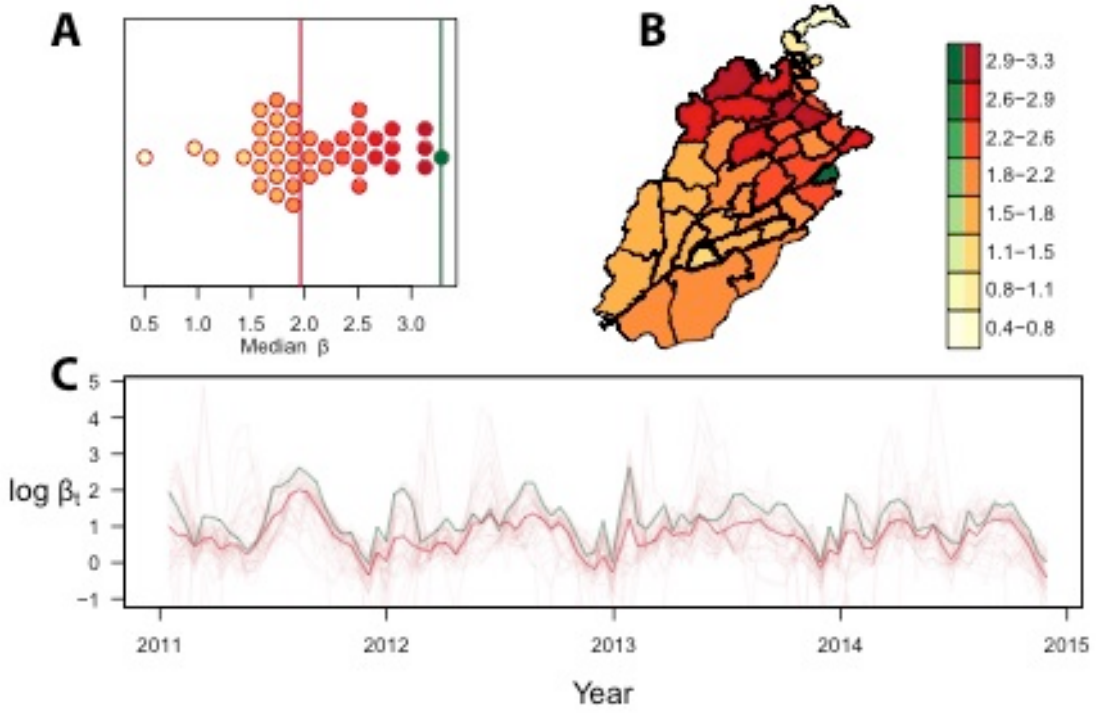

625
626

Figure 4: Ratio of betas (R_0) assuming equal force of infection and a difference in $\alpha_2 - \alpha_1$ of 0.2, 0.15 (green), and 0.1, form top to bottom. The straight line indicates a ratio of 1.

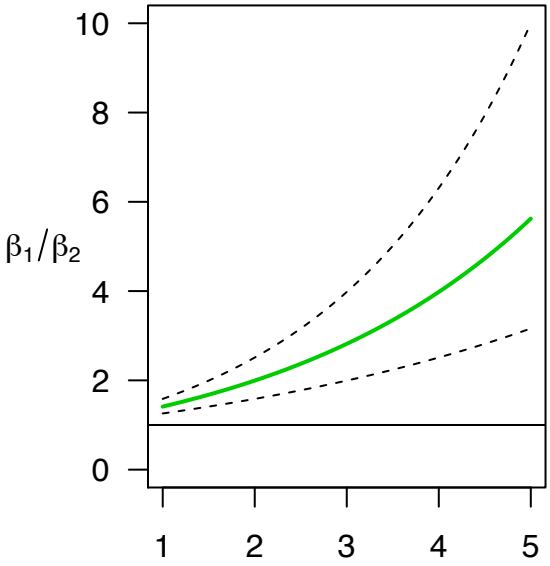

Figure 5: Critical proportion of the population to control in population 2 as a function of R_0 in population 1, the order of magnitude of the infectious numbers in each population, and a difference in $\alpha_2 - \alpha_1$ of 0.1, 0.15 (green), and 0.2. The straight line indicates the critical proportion assuming the α in each population are equal.

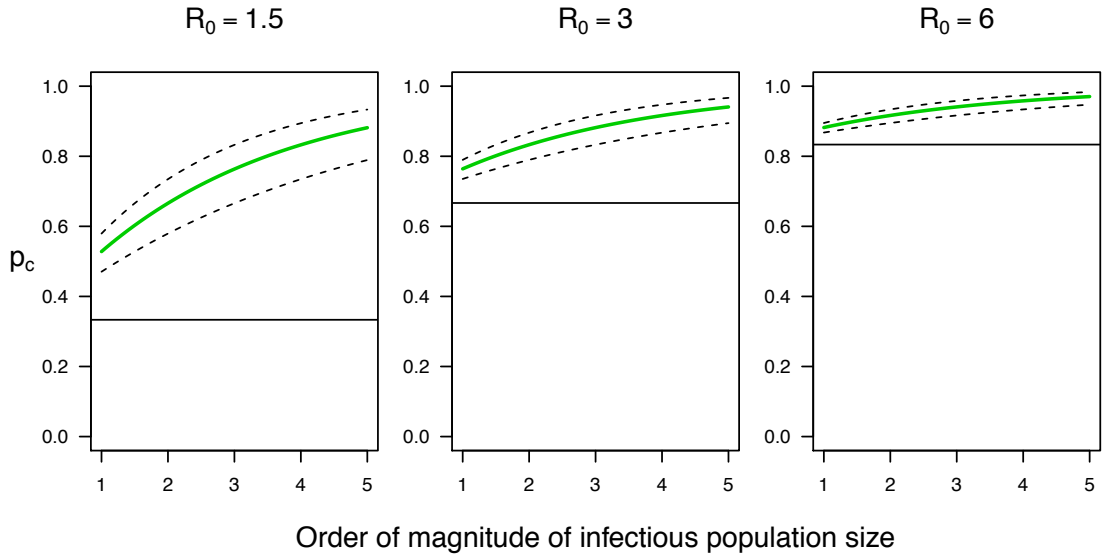

652 **Table S1: Reported case numbers per year for each district of the study region, Punjab**
653 **Province, Pakistan.**

District	2011	2012	2013	2014	Total
Attock	7	1	0	18	26
Bagh	0	0	0	0	0
Bahawalnagar	65	0	0	0	65
Bahawalpur	65	1	40	3	109
Bhakkar	33	0	0	0	33
Bhimber	0	0	0	0	0
Chakwal	0	0	0	0	0
D. G. Khan	3	0	0	0	3
Faisalabad	981	58	125	0	1164
Gujranwala	61	0	0	0	61
Gujrat	0	24	0	0	24
Hafizabad	1	0	0	0	1
Jhang	6	0	0	0	6
Jhelum	75	0	0	33	108
Kasur	77	0	0	0	77
Khanewal	2	0	0	1	3
Khushab	37	0	0	0	37
Kotli	0	0	0	0	0
Lahore	18020	4013	11516	1799	35348
Leiah	27	1	0	0	28
Lodhran	0	0	0	0	0
Mandi Bahauddi	4	0	3	0	7
Mianwali	6	0	0	0	6
Mirpur	0	0	0	0	0
Multan	371	1	64	4	440
Muzaffarabad	0	0	0	0	0
Muzaffargarh	0	0	0	0	0
Narowal	26	2	0	0	28
Neelum	0	0	0	0	0
Okara	126	3	0	0	129
Pakpattan	179	5	0	0	184
Poonch	0	0	0	0	0
Rahim Yar Khan	0	0	0	0	0
Rajanpur	0	0	0	0	0
Rawalpindi	736	132	1845	2532	5245
Sahiwal	69	4	3	0	76
Sargodha	14	0	0	0	14
Sheikhupura	29	3	42	179	253
Sialkot	49	0	0	0	49
Sudhnoti	0	0	0	0	0
Toba Tek Singh	7	1	6	2	16
Vehari	106	264	228	18	616

654

Table S2: Environmental model: no variation in α.

Term	Estimate	Std. Error	t-value	p-value
Intercept	**2.51**	**0.679**	**3.696**	**0.00028**
α	**0.690**	**0.040**	**17.288**	**< 2e-16**
EVI (yearly average)	**-8.78**	**2.499**	**-3.392**	**0.00082**
Ae. albopictus	**2.28**	**0.544**	**4.196**	**3.93e-5**
Precipitation (yearly average)	**-0.021**	**0.0079**	**-2.590**	**0.0102**
Term	**edf**	**Ref. df**	**F**	**p-value**
"Seasonality"	**3.44**	**8.00**	**1.566**	**0.0034**
Temperature	**7.55**	**8.47**	**2.537**	**0.0102**
2-week lagged temperature	**5.47**	**6.67**	**2.300**	**0.0304**
EVI	**1.83**	**2.33**	**3.373**	**0.0299**

674 **Table S3: Environmental model: α in Lahore differs from other districts.**

675

Term	Estimate	Std. Error	t-value	p-value
Intercept	**2.548**	**0.676**	**3.769**	**0.0002**
α (Lahore)	**0.741**	**0.043**	**17.088**	**<2e-16**
α (Not Lahore)	**0.594**	**0.055**	**10.887**	**<2e-16**
EVI (yearly average)	**-7.636**	**2.527**	**-3.022**	**0.003**
Ae. albopictus	**1.159**	**0.679**	**1.708**	**0.089**
Precipitation (yearly average)	**-0.008**	**0.009**	**-0.870**	**0.385**
Term	**edf**	**Ref. df**	**F**	**p-value**
"Seasonality"	**3.238**	**8.000**	**1.278**	**0.0095**
Temperature	**7.502**	**8.435**	**3.195**	**0.0016**
2-week lagged temperature	**5.866**	**7.067**	**2.371**	**0.0231**
EVI	**2.179**	**2.784**	**3.690**	**0.0154**

676

677

678

679

680

681

682

683

684

685

686 **Table S4: Full model: no variation in α.**

687

Term	Estimate	Std. Error	t-value	p-value
Intercept	**-34.83**	**9.803**	**-3.553**	**0.00047**
α	**0.578**	**0.0451**	**12.824**	**<2e-16**
EVI (yearly average)	**-60.12**	**15.04**	**-3.998**	**8.71e-5**
NDVI (yearly average)	**0.0383**	**0.0103**	**3.737**	**0.00024**
Ae. albopictus	**2.745**	**1.028**	**2.669**	**0.00826**
Weighted Access	**2.742e-5**	**6.464e-6**	**4.242**	**3.26e-5**
Urbanicity	**-2.468**	**0.9494**	**-2.600**	**0.00776**
Precipitation (yearly average)	**-0.0684**	**0.0185**	**-3.697**	**0.00028**
Term	**edf**	**Ref. df**	**F**	**p-value**
"Seasonality"	**4.480**	**8.000**	**4.173**	**3.97e-7**
Temperature	**7.607**	**8.504**	**4.396**	**4.14e-5**
2-week lagged temperature	**4.823**	**5.981**	**3.793**	**0.0013**

688

689 **Table S5: Full model: α in Lahore differs from other districts.**

690

Term	Estimate	Std. Error	t-value	p-value
Intercept	**-35.92**	**9.93**	**-3.618**	**0.00037**
α (Lahore)	**0.612**	**0.0643**	**8.510**	**<2e-16**
α (Not Lahore)	**0.555**	**0.0566**	**9.802**	**<2e-16**
EVI (yearly average)	**-61.59**	**15.19**	**-4.055**	**6.95e-5**
NDVI (yearly average)	**0.0395**	**0.010**	**3.8**	**0.00019**
Ae. albopictus	**2.81**	**1.033**	**2.721**	**0.0070**
Weighted Access	**2.42e-5**	**7.86e-6**	**3.072**	**0.0024**
Urbanicity	**-2.33**	**0.9697**	**-2.403**	**0.0171**
Precipitation (yearly average)	**-0.069**	**0.0186**	**-3.733**	**0.00024**
Term	**edf**	**Ref. df**	**F**	**p-value**
"Seasonality"	**4.350**	**8.000**	**3.817**	**1.31e-6**
Temperature	**7.620**	**8.511**	**4.335**	**4.97e-5**
2-week lagged temperature	**4.764**	**5.916**	**3.680**	**0.00178**

691

692 **Figure S1: Predicted versus expected values for α in Lahore (green) and all other**
693 **districts (red) for the environmental model.**
694

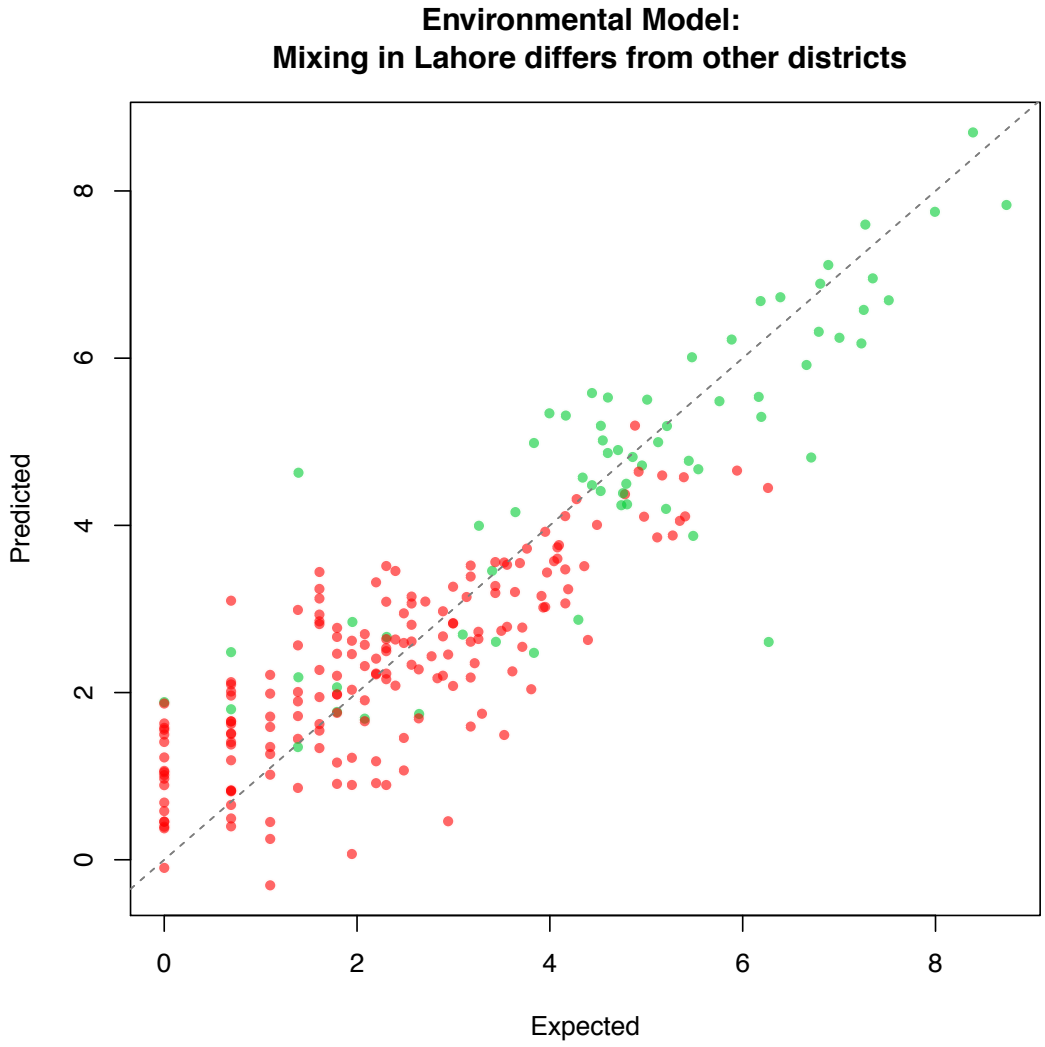

695
696 **Additional information about collection of epidemiological data.**
697 Secondary data from hospital records were used from Punjab province in Pakistan. The data
698 was initially collected by Punjab Health Department as part of the dengue prevention and
699 eradication program. For ensuring accurate reporting from the health facilities, Punjab Health
700 Department used the following three procedures: (i) Clinical case reporting, (ii) Lab case
701 reporting, and (iii) Case management. All health facilities were liable to record the data and
702 share them with Punjab Information Technology Board (PITB) within 24 hours. For clinical case
703 reporting, as per Dengue Expert Advisory Group (DEAG), guidelines, dengue suspects,
704 probable, and confirmed cases needed to be correctly entered on the PITB dashboard within
705 24 hours of admission. For lab case reporting, all private sector labs must send reports of

706 positive dengue cases in the line list format to the respective Executive District Officer Health
707 (EDOH) for online entry on the dashboard, again within 24 hours. For case management, the
708 healthcare facilities are liable to mange dengue cases regularly in specified Dengue care units,
709 OPDs, emergency units, or wards.